Cryogenic Characterization of the FBK NUV-HD SiPMs

Fabio Acerbi, Stefano Davini, Alessandro Ferri, Cristiano Galbiati, Graham Giovanetti, Alberto Gola, George Korga, Andrea Mandarano, Marco Marcante, Giovanni Paternoster, Claudio Piemonte, Alessandro Razeto, Veronica Regazzoni, Davide Sablone, Claudio Savarese, Gaetano Zappalá, and Nicola Zorzi

arXiv:1610.01915v1 [physics.ins-det] 6 Oct 2016

***Abstract*—We report on the characterization of the NUV-HD SiPMs developed at FBK at cryogenic temperature. A dedicated setup was built to measure the primary dark noise and correlated noises of the SiPMs between 40 and 300 K. Moreover a specific analysis program in conjunction with an ad-hoc data acquisition system were developed to allow the precise characterization of these parameters, some of which can vary up to 7 orders of magnitude between room temperature and 40 K. We proved that it is possible to operate the FBK NUV-HD SiPMs at temperatures lower than 100 K with a dark noise below 0.01 cps/mm^2 and total correlated noise below 35% at 6 V of over-voltage. These results are relevant for the development of future cryogenic particle detector based with SiPMs as photosensors.**

***Index Terms*—Silicon Photomultiplier, Avalanche Photodiode, Cryogenics, Dark noise, Crosstalk, Afterpulsing.**

I. Introduction

THE use of silicon photomultipliers (SiPMs) technology at cryogenic temperatures is a new line of development of increasing interest in a wide range of scientific fields. SiPMs operation at cryogenic temperature offers a very interesting option for future particle detectors, where the efficiency of the detection of scintillation light is of primary importance.

Building on its strong line of development of SiPMs [1], [2], [3], FBK developed a new generation of Near Ultra Violet - High Density (NUV-HD) SiPMs [4], whose performances make them a robust technology candidate to equip the new dark matter multi-ton detector of the DarkSide [5] collaboration with a sensitive area of about $14\,\mathrm{m}^2$ in liquid argon.

A detailed review of the performance of NUV-HD SiPMs can be found in [4]. In this article we focused on the NUV-HD SiPMs cryogenic performance relative to the dark count rate (DCR) and the correlated noises. We characterized two variants of the NUV-HD SiPMs, *i.e.* the NUV-HD Standard-Field (NUV-HD-SF) and the NUV-HD-LF Low-Field (NUV-HD-LF), which differ for the strength of the field in the avalanche region [6]. The size of all SiPMs under test is $5 \times 5\,\mathrm{mm}^2$ with SPAD cell size of $25 \times 25\,\mu\mathrm{m}^2$.

We developed a cryogenic test setup equipped with a flexible data acquisition system and an ad-hoc analysis tool, suitable for the characterization of SiPMs and SiPMs assemblies in the temperature range from $40\,\mathrm{K}$ to $300\,\mathrm{K}$.

The second section is devoted to the cryogenic experimental setup. The third and fourth sections introduce, respectively, the data acquisition system and the analysis tool. In the fifth section, we detail the results obtained on the NUV-HD SiPMs.

II. Cryogenic Setup

The cryogenic setup is contained in a stainless steel vacuum chamber made of a cylindrical tube of $500\,\mathrm{mm}$ length closed by two DN 320 ISO-K flanges. Inside the vacuum chamber sits a PTFE thin cylinder, shielded by a layer of superinsulator, which serves as a thermal shield. The cryostat is equipped with a set of vacuum bulkhead feedthroughs: coaxial SMA connections are reserved for the SiPM signal, while a set of hermetic high density connectors are used for temperature readout, power load,

Manuscript created October 4, 2016.

The development of the NUV-HD and NUV-HD-LF SiPM technologies was funded by the EU FP7 project SUBLIMA, Grant 241711. We acknowledge support from NSF (US, Grant PHY-1314507 for Princeton University), the Istituto Nazionale di Fisica Nucleare (Italy) and Laboratori Nazionali del Gran Sasso (Italy).

S. Davini, A. Mandarano, and C. Savarese are with Gran Sasso Science Institute, L'Aquila 67100, Italy and INFN Laboratori Nazionali del Gran Sasso, Assergi (AQ) 67100, Italy.

F. Acerbi, A. Ferri, A. Gola, C. Piemonte and N. Zorzi are with Fondazione Bruno Kessler, Povo 38123, Italy and Trento Institute for Fundamental Physics and Applications, Povo 38123, Italy.

M. Marcante, V. Regazzoni, G. Zappalá are with Fondazione Bruno Kessler, Povo 38123, Italy, Trento Institute for Fundamental Physics and Applications, Povo 38123, Italy and Physics Department, Università degli Studi di Trento, Povo 38123, Italy.

C. Galbiati is with Physics Department, Princeton University, Princeton, NJ 08544, USA.

G. Korga is with Department of Physics, University of Houston, Houston, TX 77204, USA and INFN Laboratori Nazionali del Gran Sasso, Assergi (AQ) 67100, Italy.

G. Giovanetti, A. Razeto and D. Sablone are with INFN Laboratori Nazionali del Gran Sasso, Assergi (AQ) 67100, Italy and Physics Department, Princeton University, Princeton, NJ 08544, USA.

Corresponding Author: sarlabb7@lngs.infn.it

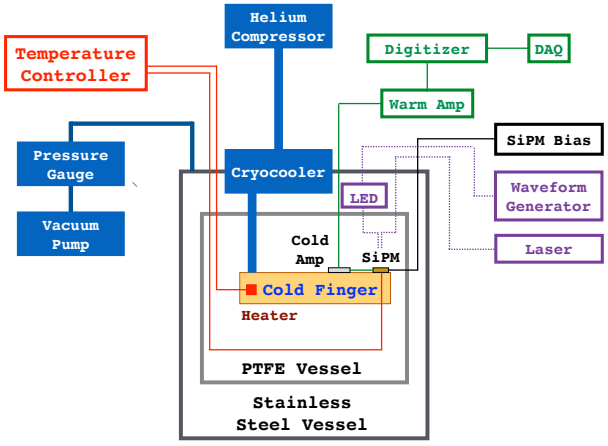

Fig. 1. Sketch of the experimental setup.

pre-amplifier voltage supply and bias. An optical fiber hermetic feedthrough is installed to illuminate the device under test from a laser source; a blue LED is installed in the cryostat for the same reason. To minimize the light leaks, which could spoil the dark rate measurements, a small dark box was built to contain the SiPM, as described later in this section. Furthermore, a blackout fabric is wrapped around the cryostat to reduce even more the light entering the chamber. An overall sketch of the system is shown in Fig. 1.

During operations, the chamber reaches a vacuum level of about 10^{-2} mbar thanks to a Pfeiffer ACP15 multi-stage roots evacuation pump. A Cryomech PT90 pulse tube cryocooler, capable of delivering 90 W of cooling capacity at 77 K, is mounted on the top of the DN 320 ISO-K flange. The cold head of the cryocooler is equipped with a cold finger, which holds the SiPM assembly under test as shown in Fig. 2. This arrangement allows for a fast thermal cycle: the cold finger can be thermalized from room temperature to 40 K in about 40 min. The cold finger also hosts a platinum RTD, in SMD package, soldered to the Printed Circuit Board (PCB) and connected via low thermal conductance phosphor bronze wires to a Lakeshore 335 temperature controller, which drives the thermal load required for temperature regulation directly to a set of high power metal film resistors mounted on the cold finger. This system has proven to reach a temperature stability of about 0.1 K and an accuracy of about 3 K in the range of interest 40 K to 300 K. A Lakeshore 218 meter measures the temperature of other platinum RTD sensors installed in the cryostat.

To minimize unwanted thermal gradients, the SiPM holders, shown in Fig. 3, are realized in 1.6 mm-thick aluminum PCB using Insulated Metallic Substrate (IMS) technology, to which the SiPM sample is bonded with the silver-loaded conductive epoxy Master-Bond EP21TDCS-LO. The holder is firmly connected to

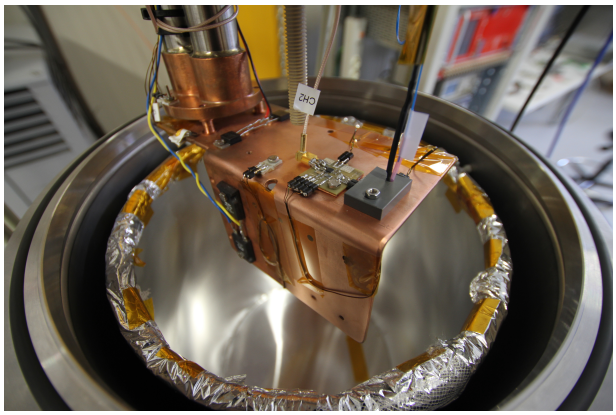

Fig. 2. Detail of the cold finger, positioned just above the top opening of the stainless steel cylindrical tube. Also visible is the PTFE tube covered by the superinsulator. On the right hand side of the cold finger, a black box contains the SiPM under test. Two unjacketed optical fibers, connected to a LED and to a laser source placed outside the vacuum chamber, penetrate the top side of the black box, delivering calibrated light signals to the SiPM under test. In the center of the cold finger is a cryogenic pre-amplifier, and on the left are the cold head of the cryocooler and the set of high power film resistors in use to control temperature.

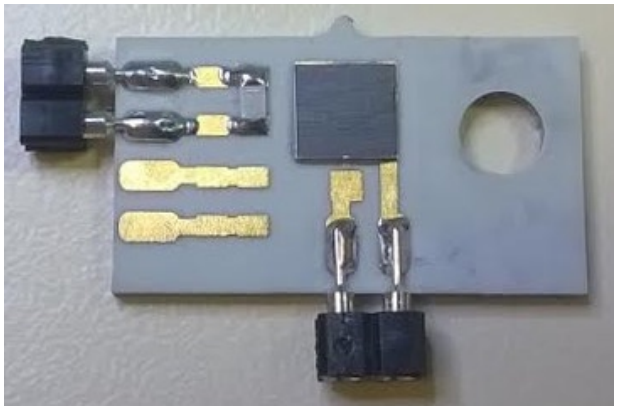

Fig. 3. The SiPM holder is a custom aluminum PCB realized with IMS technology. The FBK SiPM is visible at the center of the PCB. On the left corner the SMD platinum RTD is visible.

the cold finger by a screw, with a thin layer of cryogenic grease ensuring a good thermal contact between the copper and the aluminum board. A cryogenic pre-amplifier specifically designed for this application is connected to the SiPM and is in thermal equilibrium with the cold finger.

III. Readout Chain and Data Acquisition System

The readout chain is composed by:

- a SiPM bias source, feeding the SiPM from outside the cryostat;
- a cryogenic pre-amplifier, directly connected to the device under test, and its bias source;

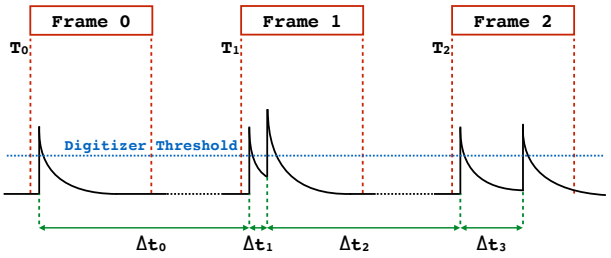

Fig. 4. Schematic representation of the capture of SiPM waveforms in different frames. Each frame can capture one or more SiPM pulses. See the text for details on calculation of the inter-arrival time between pulses in different frames.

- a low noise warm amplifier, receiving the signal from the pre-amplifier outside the cryostat;
- a high speed digitizer.

A Keithley 2450 SourceMeter is used to provide the bias voltage to the SiPM. This unit can directly measure the current-voltage (IV) curves of the SiPM both in forward and reverse polarity with a 1 nA resolution, allowing a precise measurement of the temperature-dependent values for the breakdown voltage of the SPAD cells and for the resistance of the quenching resistor.

The cryogenic pre-amplifier is provided by a high speed, low noise operational amplifier configured as trans-impedance amplifier (TIA), with a feedback resistor of 500 Ω providing a gain of 0.5 mV/µA. This configuration allows a reasonable sensitivity even considering the very large SiPM input capacitance of 50 pF/mm^2. The pre-amplifier includes a resistor of 20 Ω between the SiPM and the TIA: the benefits of this series resistor include both a reduction of the noise gain at high frequencies and a better matching of the signal from the SiPM with the amplifier avoiding undershoots [7]. The design and the implementation of the cryogenic pre-amplifier will be discussed in a future publication.

The warm amplifier consists of a single stage non-inverting amplifier based on a high speed, low noise operational amplifier, model *OPA847* from *Texas Instruments*. The resulting input noise equivalent is 11 µV, significantly smaller than the output noise from the cryogenic pre-amplifier. The device is configured for a gain of 28.8 V/V with a rise time of 7 ns.

The power supply for both the cryogenic pre-amplifier and the warm amplifier is provided by two Elind 32DP8 units.

The amplified signal is fed into a channel of a CAEN V1751 1 GS/s 10 bit digitizer, configured for interleaved acquisition and operated in auto-trigger mode, recording data for a fixed gate when the digitized signal crosses a fixed threshold. A custom C++ program handles the configuration and the readout of the digitizer. Data are saved in a custom file format, with each frame in the file including the digitized waveform and a header,

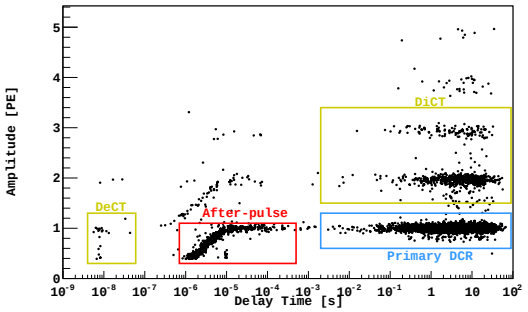

Fig. 5. Distribution of delay time versus amplitude for run at 77 K and in absence of light stimulation. A few components of the noise response of the SiPM can be clearly identified: primary dark count (part of the Dark Count Rate, DCR), Direct CrossTalk (DiCT), Delayed CrossTalk (DeCT), and AfterPulsing (AP).

which contains accurate timing information – see Fig. 4.

Two time stamps, a fine and a coarse counter, are saved for each frame. The first is obtained directly by the digitizer and represents the starting time of each frame, counting from the beginning of the measurement. It has a resolution of 8 ns and an overflow time of roughly 37 s. In order to recover the time information when the acquisition time exceeds the overflow, as this can easily be the case with the low event rate expected at cryogenic temperature, an additional coarse counter is extracted by the operating system of the computer, with a lower precision (of the order of 10 ms).

The trigger threshold value is set by the user depending on the device under test, the noise level and the signal gain, but it's usually set to be half of the value of the single cell response. The length of the acquisition gate depends on the pulse rate from the SiPM. At cryogenic temperatures, the low rate enables the use of a short, 10 µs gate, typically recording a single SiPM pulse. Near room temperature, the gate is normally set to 2 ms, which allows to record many pulses in the same gate. In this case, time differences between consecutive pulses are evaluated from the analysis of the waveform only.

IV. The Data Analysis Software

The data analysis software was developed at FBK following the procedure described in [8]. It reads the data stored in the data frames and performs a detailed analysis of SiPMs response, with special emphasis on the time correlation of pulses. The analysis capabilities are strongly enhanced by the addition of the time tagging of frames previously described in Sec. III, which is mandated by the significant difference in SiPM dark pulse rates as a function of temperature, which spans several orders of magnitude. The time tagging of frames allows to calculate the time difference between consecutive pulses from the nanosecond scale using pulses within the same frame, up to thousands of seconds

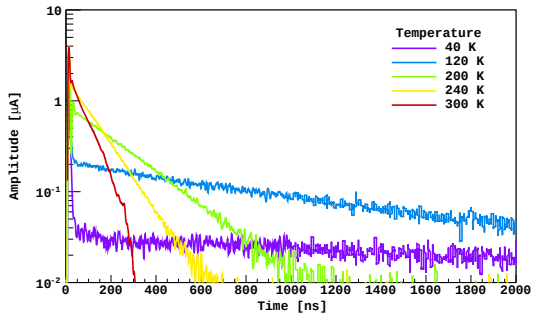

Fig. 6. Average of NUV-HD-LF SCR at different temperatures and at the same over-voltage. The presence of two components at all temperatures is evident, as well as the increase of the SPAD recharge time with decreasing temperatures. A similar behavior is observed with NUV-HD-SF SiPMs.

using different frames, with the only practical limit set by the time available for measurement. This allows a seamless determination of the temperature-dependent SiPM pulse rate, a detailed study of their correlation, and the extraction of the secondary noise probabilities.

For data collected near room temperature, the frame time tag is not helpful, as each frame may already contain several hundreds of events and the dead time required by the digitizer to store the data becomes comparable with the inverse of the dark rate. Except for this difference in the utilization of data, the analysis is uniform for all types of dataset: each event is tagged with an ordered pair of values, *i.e.* the time distance from the previous pulse and the amplitude. A typical scatter plot with all ordered pairs recorded for a run at 77 K and in absence of light stimulation is shown in Fig. 5. The plot allows to identify different kind of pulses, composing the noise response of the SiPM.

DCR: The main group of events is determined by primary, Poisson-distributed, dark counts that make up Dark Count Rate, DCR. The amplitude is centered at around 1 PE, and the distribution in time distance is an exponential with decay time corresponding to the inverse of the DCR.

DiCT: Direct CrossTalk (DiCT) events occur in a very short time difference given by the travel time needed by the crosstalk photon to reach a neighboring cell and trigger an independent avalanche: the time required is in the picosecond time scale, nearly impossible to be resolved with the readout electronics at hand. As a result, DiCT pulses are superimposed to DCR pulses, have a similar time distribution, but are characterized by greater amplitudes, corresponding to the detection of 2 or more PE.

DeCT: The less populated groups with characteristic delay time of few to tens of nanoseconds are instead due to Delayed CrossTalk (DeCT). These events are caused by crosstalk photons absorbed in the non-depleted region of a neighboring cell. The carriers diffuse for a short time before reaching the high-field region and finally triggering an avalanche. The resulting pulse has the single cell amplitude but is delayed with respect to the previous by the characteristic diffusion time, typically in the order of few to tens of nanoseconds. Such delayed pulses can further trigger DiCT pulses, yielding to events with the same time distribution but higher amplitudes.

AP: Finally, the group of events with intermediate delay times and amplitude of 1 PE or lower than are identified as AfterPulsing (AP). Afterpulsing occurs when, during an avalanche, an electron is trapped by some impurity in the silicon lattice and is then released after a characteristic time, generating a second avalanche. Since the afterpulsing event and its primary avalanche occur in the same cell, the time distribution is determined by both the trap(s) time constant(s) and the recharge time constant of the microcell. When the time distance is lower than the full micro-cell recharge, the resulting pulse has a reduced amplitude. As with the other types of events, they can trigger DiCT pulses, explaining the higher amplitude groups with the same time distribution.

At the end of the analysis stage the following parameters are saved: primary DCR, correlated noise probabilities (DiCT, DeCT, AP), single cell signal features (amplitude, recovery time, charge delivered in a fixed time gate). Also stored is the waveform resulting from the application of the Differential Leading Edge Discriminator (DLED) algorithm, as defined in [9], which turns useful for the evaluation of the breakdown voltage, as the resulting peak amplitude is linear with the applied over-voltage. Consideration of the DLED amplitude as a function of over-voltage typically allows a more precise determination of V_{BD} than what is possible to derive from the IV curve. This method allows to determine precisely the over-voltage as a function of temperature. In order to compare the SiPM DCR as a function of temperature, it is important that each point be taken at the same over-voltage. Therefore, any plot of DCR vs. over-voltage is re-corrected in the analysis stage, by performing a linear interpolation over the data to extract the correct DCR at the exact value of over-voltage as determined with this procedure. The same consideration applies for all the other SiPM features.

V. Experimental Results

The Single Cell Response (SCR) is defined as the signal generated at the output of the amplifier when a single microcell of the SiPM fires. All devices under test are passively quenched with a polysilicon resistor, whose quenching resistance is denoted with R_q. The impedance of this material depends strongly on temperature, increasing with decreasing temperature, therefore affecting various signal features. The typical SiPM pulse is made

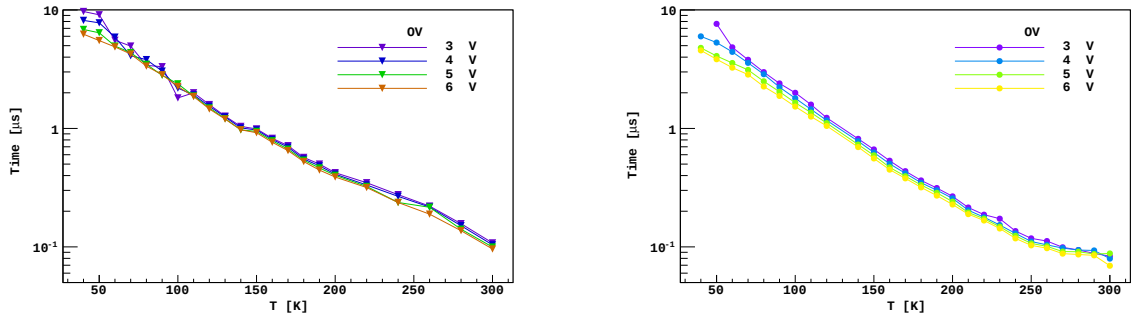

Fig. 7. SPAD recharge time constant for NUV-HD-SF (left) and NUV-HD-LF (right) SiPMs as a function of over-voltage and temperature.

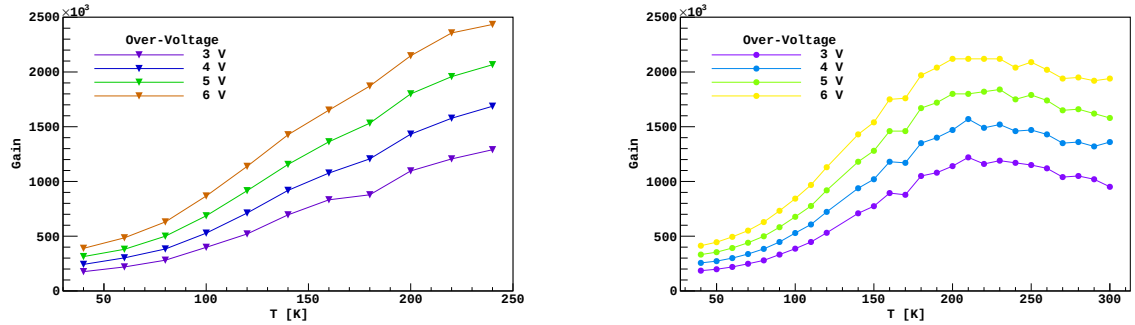

Fig. 9. Gain of the NUV-HD-SF (left) and NUV-HD-LF (right) SiPMs as a function of over-voltage and temperature.

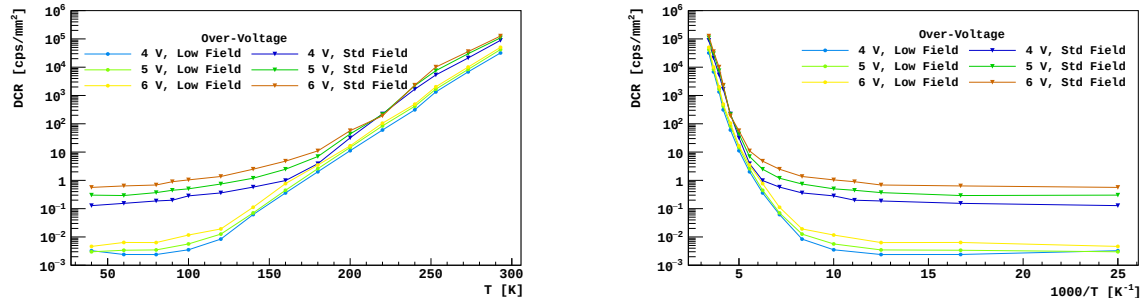

Fig. 10. **Left:** DCR for NUV-HD-SF (triangular markers) and NUV-HD-LF (circular markers) devices as function of over-voltage and temperature. **Right:** the same data plotted as a function of $1/T$, which allows to distinguish two generation mechanisms of DCR pulses, *i.e.* the thermal signals which drop exponentially for increasing $1/T$ and the tunneling signals responsible for the residual rate in the plateau region.

up of two different components: a fast component, whose time constant τ_f is of the order of few nanoseconds, and a slow component, whose time constant τ_s can extend to several microseconds, this time constant corresponding to the SPAD recharge time. The electric model proposed in [10] is well suited to describe the SiPM behaviour: the slow time constant is expected to be proportional to the quenching resistance as in $\tau_s = R_q \cdot (C_{\mathrm{SPAD}} + C_q)$, where C_q is the parasite capacitance of the polysilicon resistor. With decreasing temperature, the increase in R_q translates in higher values of τ_s. This effect can be easily appreciated in Fig. 6.

The analysis program described previously in Sec. IV allows to fit the recharge (recovery) time for the individual SPAD as a function of over-voltage and temperature. The result is shown in Fig. 7: NUV-HD-SF and NUV-HD-LF SiPMs exhibit the same exponential trend, with a slight difference in overall results.

The peak amplitude of the SCR is mainly determined by the fast peak. Its amplitude increases linearly with over-voltage and only very slowly with temperature (see Fig. 8).

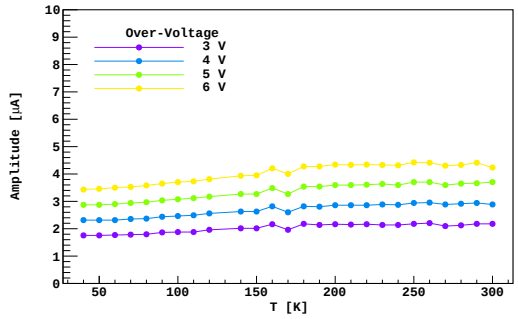

Fig. 8. Amplitude of the average SPAD response as function of over-voltage and temperature.

For each pulse, the overall charge released (hence the gain) is measured by comparing the result of the integration of the signal in two fixed and equal gates: one containing the pulse and a second right before it. By measuring the distance between the peaks of the resulting distributions and considering the amplification factors it is possible to calculate the number of carriers generated in the SPAD. Again the two variants of the NUV-HD technology show similar results, see Fig. 9. The variation with temperature is due to the fact that, with decreasing temperature and longer pulses, an increasingly larger fraction of the total pulse sits out of the 500 ns integration gate. Near room temperature, when the signal duration becomes shorter than the integration time, the gain is expected to saturate to a plateau: the residual dependence on temperature observed is due to the variation with temperature of the depletion width of each SPAD for a given over-voltage. This happens because the breakdown voltage changes with temperature as well. Therefore, we also observe a variation of the SPAD junction capacitance and thus of its gain.

The NUV-HD-LF SiPMs are especially optimized to achieve good performances in terms of DCR reduction at low temperature. They exhibit a DCR that is one to two orders of magnitude lower than the NUV-HD-SF at the same value of over-voltage, see Fig. 10. The visualization of the DCR over the entire temperature range of interest in form of an Arrhenius plot, see Fig. 10, allows to distinguish between the two different mechanisms responsible for the dark rate generation: thermal generation dominates at high temperatures [11], [12], while at low temperature the main contribution originates from tunneling [13]; due to the lower electric field value, the magnitude of the latter component is highly suppressed in NUV-HD-LF SiPMs.

The NUV-HD-LF SiPMs present lower correlated noises with respect to the NUV-HD-SF SiPMs at the same OV, see Fig. 11, 12. This is explained with the overall lower gain and avalanche triggering probability in the NUV-HD-LF devices. The DiCT exhibits only a weak dependence on the temperature, while it is linear in over-voltage, see Fig. 11. The difference between the two technologies performances in the AP probability cannot be ascribed only to the lower gain of the devices, but probably also to a suppression of some field effects contributing to this noise component. Both AP and DeCT (whose probability is very low in both technologies, see Fig. 13) reach a maximum in the temperature range from 60 K to 80 K and then decrease to zero in the high temperature region. This peculiar dependence can be explained by the interplay of two different phenomena having opposite effects on the noise probability: at low temperatures the trapping time constants increase, enhancing the probability of a carrier to be released when the cell is at least partially recharged, producing an AP event; on the other hand, the quenching resistance grows exponentially (see Fig. 7), thus suppressing the avalanche triggering probability during the recharge. Similarly, for DeCT the lifetime of the charge carriers in the bulk of the SiPM increases at low temperatures, boosting their chances to diffuse till the high field region, while the increase of the quenching resistance has the same effect explained for the AP.

VI. Conclusions

We developed a cryogenic setup, equipped with a robust data acquisition system, suitable for a broad variety of tests on SiPMs as a function of temperature in the interval 40 K to 300 K. This system is complemented with a comprehensive analysis software, developed on the basis of a set of tools largely used at FBK and optimized to work in a wide range of count rates. The NUV-HD-LF SiPMs performance at cryogenic temperature is impressive, with a DCR as low as 0.01 cps/mm^2. The NUV-HD-LF SiPMs are a strong candidate for the technology of choice of future particle detectors. Further design work for the optimization of the value the quenching resistor as well as for the further reduction of the field in the avalanche region (and consequently of the DCR) is ongoing at FBK. Measurements of the PDE of the NUV-HD are ongoing, as well as a full cryogenic characterization of the FBK RGB-HD family of SiPMs.

References

[1] C. Piemonte, "A new Silicon Photomultiplier structure for blue light detection," *Nucl. Inst. Meth. A*, vol. 568, no. 1, pp. 224–232, Nov. 2006. [Online]. Available: http://linkinghub.elsevier.com/retrieve/pii/S016890020601271X

[2] N. Dinu, R. Battiston, M. Boscardin, G. Collazuol, F. Corsi, G. F. Dalla Betta, A. Del Guerra, G. Llosá, M. Ionica, G. Levi, S. Marcatili, C. Marzocca, C. Piemonte, G. Pignatel, A. Pozza, L. Quadrani, C. Sbarra, and N. Zorzi, "Development of the first prototypes of Silicon PhotoMultiplier (SiPM) at ITC-irst," *Nucl. Inst. Meth. A*, vol. 572, no. 1, pp. 422–426, Mar. 2007. [Online]. Available: http://linkinghub.elsevier.com/retrieve/pii/S0168900206021462

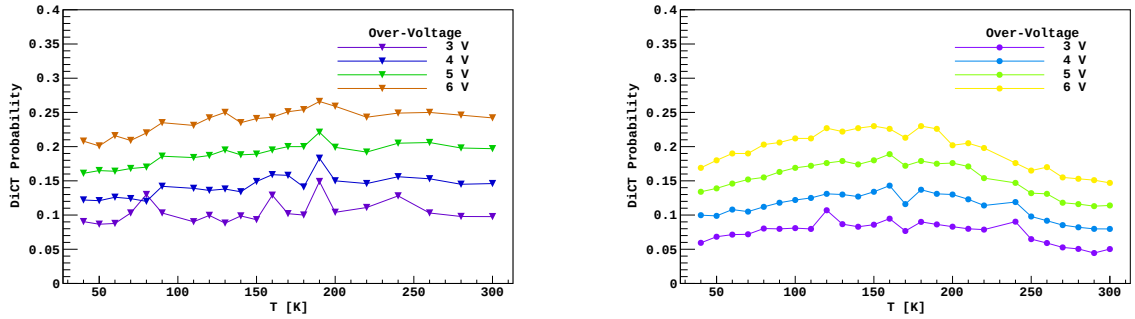

Fig. 11. DiCT probability as function of temperature for different over-voltage for for NUV-HD-SF (left panel) and NUV-HD-LF (right panel) SiPMs. DiCT values are similar for the two technologies and exhibit a weak dependence on temperature.

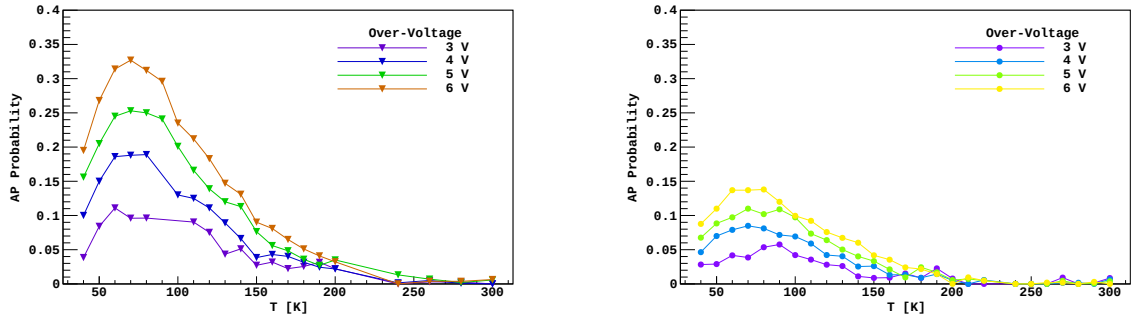

Fig. 12. AP probability as function of temperature for different over-voltage for NUV-HD-SF (left panel) and NUV-HD-LF (right panel) SiPMs. AP is significantly lower for NUV-HD-LF SiPMs.

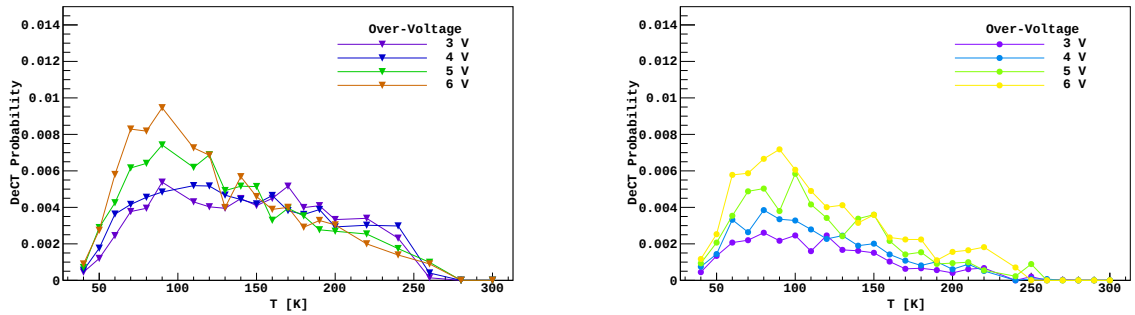

Fig. 13. DeCT probability as function of temperature for different over-voltage for for NUV-HD-SF (left panel) and NUV-HD-LF (right panel) SiPMs. DeCT is negligible for both types of SiPMs.

[3] C. Piemonte, R. Battiston, M. Boscardin, G. F. Dalla Betta, A. Del Guerra, N. Dinu, A. Pozza, and N. Zorzi, "Characterization of the First Prototypes of Silicon Photomultiplier Fabricated at ITC-irst," *IEEE Trans. Nucl. Sci.*, vol. 54, no. 1, pp. 236–244, 2007. [Online]. Available: http://ieeexplore.ieee.org/lpdocs/epic03/wrapper.htm?arnumber=4089179

[4] C. Piemonte, F. Acerbi, A. Ferri, A. Gola, G. Paternoster, V. Regazzoni, G. Zappala, and N. Zorzi, "Performance of NUV-HD Silicon Photomultiplier Technology," *IEEE Trans. Elec. Dev.*, vol. 63, no. 3, pp. 1111–1116, 2016. [Online]. Available: http://ieeexplore.ieee.org/lpdocs/epic03/wrapper.htm?arnumber=7397984

[5] P. Agnes, L. Agostino, I. F. M. Albuquerque, T. Alexander, A. K. Alton, K. Arisaka, H. O. Back, B. Baldin, K. Biery, G. Bonfini, M. Bossa, B. Bottino, A. Brigatti, J. Brodsky, F. Budano, S. Bussino, M. Cadeddu, L. Cadonati, M. Cadoni, F. P. Calaprice, N. Canci, A. Candela, H. Cao, M. Cariello, M. Carlini, S. Catalanotti, P. Cavalcante, A. Chepurnov, A. G. Cocco, G. Covone, L. Crippa, D. D'Angelo, M. D'Incecco, S. Davini, S. De Cecco, M. De Deo, M. De Vincenzi, A. Derbin, A. Devoto, F. Di Eusanio, G. Di Pietro, E. Edkins, A. Empl, A. Fan, G. Fiorillo, K. Fomenko, G. Forster, D. Franco, F. Gabriele, C. Galbiati, C. Giganti, A. M. Goretti, F. Granato, L. Grandi, M. Gromov, M. Guan, Y. Guardincerri, B. R. Hackett, K. Herner, E. V. Hungerford, A. Ianni, A. M. Ianni, I. James, C. Jollet, K. Keeter, C. L. Kendziora, V. V. Kobychev, G. Koh, D. Korablev, G. Korga, A. Kubankin, X. Li, M. Lissia,

P. Lombardi, S. Luitz, Y. Ma, I. N. Machulin, A. Mandarano, S. M. Mari, J. Maricic, L. Marini, C. J. Martoff, A. Meregaglia, P. D. Meyers, T. Miletic, R. Milincic, D. Montanari, A. Monte, M. Montuschi, M. E. Monzani, P. Mosteiro, B. J. Mount, V. N. Muratova, P. Musico, J. Napolitano, A. Nelson, S. Odrowski, M. Orsini, F. Ortica, L. Pagani, M. Pallavicini, E. Pantic, S. Parmeggiano, K. Pelczar, N. Pelliccia, S. Perasso, A. Pocar, S. Pordes, D. A. Pugachev, H. Qian, K. Randle, G. Ranucci, A. Razeto, B. Reinhold, A. L. Renshaw, A. Romani, B. Rossi, N. Rossi, S. D. Rountree, D. Sablone, P. Saggese, R. Saldanha, W. Sands, S. Sangiorgio, C. Savarese, E. Segreto, D. A. Semenov, E. Shields, P. N. Singh, M. D. Skorokhvatov, O. Smirnov, A. Sotnikov, C. Stanford, Y. Suvorov, R. Tartaglia, J. Tatarowicz, G. Testera, A. Tonazzo, P. Trinchese, E. V. Unzhakov, A. Vishneva, R. B. Vogelaar, M. Wada, S. Walker, H. Wang, Y. Wang, A. W. Watson, S. Westerdale, J. Wilhelmi, M. M. Wojcik, X. Xiang, J. Xu, C. Yang, J. Yoo, S. Zavatarelli, A. Zec, W. Zhong, C. Zhu, and G. Zuzel, "Results from the first use of low radioactivity argon in a dark matter search," *Phys. Rev. D*, vol. 93, no. 8, p. 081101, Apr. 2016. [Online]. Available: http://link.aps.org/doi/10.1103/PhysRevD.93.081101

[6] A. Ferri, F. Acerbi, A. Gola, G. Paternoster, C. Piemonte, and N. Zorzi, "Performance of FBK low-afterpulse NUV silicon photomultipliers for PET application," *JINST*, vol. 11, no. 03, pp. P03 023–P03 023, Mar. 2016. [Online]. Available: http://stacks.iop.org/1748-0221/11/i=03/a=P03023?key=crossref.3b90668de68c0dbe8d723d4154a2ece8

[7] A. Gola, C. Piemonte, and A. Tarolli, "Analog Circuit for Timing Measurements With Large Area SiPMs Coupled to LYSO Crystals," *IEEE Trans. Nucl. Sci.*, vol. 60, no. 2, pp. 1296–1302, 2013. [Online]. Available: http://ieeexplore.ieee.org/lpdocs/epic03/wrapper.htm?arnumber=6496294

[8] C. Piemonte, A. Ferri, A. Gola, A. Picciotto, T. Pro, N. Serra, A. Tarolli, and N. Zorzi, "Development of an automatic procedure for the characterization of silicon photomultipliers," *IEEE Conf. Pub.*, pp. 428–432, 2012. [Online]. Available: http://ieeexplore.ieee.org/lpdocs/epic03/wrapper.htm?arnumber=6551141

[9] A. Gola, C. Piemonte, and A. Tarolli, "The DLED Algorithm for Timing Measurements on Large Area SiPMs Coupled to Scintillators," *IEEE Trans. Nucl. Sci.*, vol. 59, no. 2, pp. 358–365, Apr. 2012. [Online]. Available: http://ieeexplore.ieee.org/lpdocs/epic03/wrapper.htm?arnumber=6175972

[10] F. Corsi, A. Dragone, C. Marzocca, A. Del Guerra, P. Delizia, N. Dinu, C. Piemonte, M. Boscardin, and G. F. Dalla Betta, "Modelling a silicon photomultiplier (SiPM) as a signal source for optimum front-end design," *Nucl. Inst. Meth. A*, vol. 572, no. 1, pp. 416–418, Mar. 2007. [Online]. Available: http://linkinghub.elsevier.com/retrieve/pii/S0168900206021449

[11] R. N. Hall, "Electron-Hole Recombination in Germanium," *Phys. Rev.*, vol. 87, no. 2, pp. 387–387, Jul. 1952. [Online]. Available: http://link.aps.org/doi/10.1103/PhysRev.87.387

[12] W. Shockley and W. T. Read, "Statistics of the Recombinations of Holes and Electrons," *Phys. Rev.*, vol. 87, no. 5, pp. 835–842, Sep. 1952. [Online]. Available: http://link.aps.org/doi/10.1103/PhysRev.87.835

[13] M. Ghioni, A. Gulinatti, I. Rech, P. Maccagnani, and S. Cova, "Large-area low-jitter silicon single photon avalanche diodes," *Proc. SPIE*, vol. 6900, pp. 69 001D–69 001D–13, Jan. 2008. [Online]. Available: http://proceedings.spiedigitallibrary.org/proceeding.aspx?doi=10.1117/12.761578